Low-Energy Energetic Neutral Atom Imaging of Io Plasma and Neutral Tori

Yoshifumi Futaana, Stas Barabash, Xiao-Dong Wang, Martin Wieser, and Gabriella S. Wieser

Swedish Institute of Space Physics, Box 812, Kiruna 98128, Sweden.

Peter Wurz

University of Bern.

Norbert Krupp

Max Planck Institute for Solar System Research.

Pontus C:son Brandt

Applied Physics Laboratory, Johns Hopkins University.

Corresponding author

Yoshifumi Futaana, Swedish Institute of Space Physics, Box 812, Kiruna 98128, Sweden.

E-mail: futaana@irf.se
Tel: +46-980-79025
Fax: +46-980-79050

Abstract

Io's plasma and neutral tori play significant roles in the Jovian magnetosphere. We present feasibility studies of measuring low-energy energetic neutral atoms (LENAs) generated from the Io tori. We calculate the LENA flux between 10 eV and 3 keV. The energy range includes the corotational plasma flow energy. The expected differential flux at Ganymede distance is typically 10^3-10^5 cm^{-2} s^{-1} sr^{-1} eV^{-1} near the energy of the corotation. It is above the detection level of the planned LENA sensor that is to be flown to the Jupiter system with integration times of 0.01–1 seconds. The flux has strong asymmetry with respective to the Io phase. The observations will exhibit periodicities, which can be attributed to the Jovian magnetosphere rotation and the rotation of Io around Jupiter. The energy spectra will exhibit dispersion signatures, because of the non-negligible flight time of the LENAs from Io to the satellite. In 2030, the Jupiter exploration mission JUICE will conduct a LENA

measurement with a LENA instrument, the Jovian Neutrals Analyzer (JNA). From the LENA observations collected by JNA, we will be able to derive characteristic quantities, such as the density, velocity, velocity distribution function, and composition of plasma-torus particles. We also discuss the possible physics to be explored by JNA in addition to the constraints for operating the sensor and analyzing the obtained dataset.

1. Introduction

1.1 Io neutral and plasma tori

Io, the innermost Galilean moon of Jupiter, introduces a large amount material of volcanic origin to the Jovian magnetosphere. As a result, the Jovian magnetosphere is composed of heavy ions (oxygen, sulfur, and their compounds). The strong and localized source of particles near Io creates characteristic spatial distributions of plasma and neutral particles in the Jovian magnetosphere, namely, the Io neutral and plasma tori (see, for example, reviews by Dessler 1983; Thomas et al. 2004; Schneider and Bagenal, 2007; and references therein).

The Io neutral torus (called also as neutral cloud) is a dense concentration of atoms and molecules of volcanic origin that has formed around the Io orbit. These atoms are gravitationally bound to Jupiter. The composition is mainly sulfur (S) and oxygen (O) atoms as well as their compounds (e.g. Thomas et al., 2004). Hydrogen (H) atoms also exist, but the fraction thereof is small. Sodium (Na) atoms are also present. Na is bright because of its D-lines, but the fraction thereof is quite small; therefore the Na imaging is considered as a trace gas of more abundant compositions in the neutral torus (Mendillo et al., 2004). These atoms form a partial ring-like shape, which is associated with the short time scale of the loss of atoms via ionization (a few hours to 10s of hours depending on the processes; see e.g. Schneider and Bagenal., 2007) compared to the filling time of the full torus (~150 hours assuming 2.5 km/s, the escape velocity of Io).

When the neutral components in the Io neutral torus are ionized, the charged particles are accelerated by the motional electric field in the corotational flow in the magnetosphere. The accelerated ions form a plasma torus. The main components are (singly or multiply) charged O ions and S ions. H^+ ions are also present but the fraction thereof is less abundant. It is often assumed 10% [e.g. Thomas et al. 2004]. However, there are several measurements showing much smaller fraction than 10% (e.g. Wang et al., 1998a, b; Zarka et al., 2001). The plasma in the torus is corotating with the Jovian magnetosphere. At the Io orbit, the corotational velocity of the plasma is ~74 km/s. The revolution speed of Io is ~17 km/s in the same direction as the corotational flow, so the relative plasma flow velocity is ~57 km/s (e.g. Thomas et al., 2004). Even though the plasma source is more localized, because of the longer residence time (Schneider and Bagenal, 2007) compared with the rotation of the Jovian magnetosphere (9.925 hour) the plasma torus is nearly axisymmetric in a plane, referred to as the centrifugal equator (Hill 1974), defined by the rotation and magnetic dipole tilt. The tilt of the magnetic dipole is ~9.6° (according to the so-called O4 model; Acuña and Ness, 1976), while that of the centrifugal equator is represented as 2/3 of the magnetic tilt (Hill 1974).

After the Io neutral torus was discovered via the D-line emission of Na (Brown 1974) and Io plasma torus via S+ emission (Kupo et al., 1976), many observations on Io tori have been performed. Historically, investigations of the Io tori have been conducted via UV and IR spectroscopy (Herbert et al., 2001; Mendillo et al, 2004; Nozawa et al., 2004; Steffl et al., 2004a; 2004b; 2006; 2008; Yoneda et al., 2010; 2014) and in situ plasma observations (Bagenal., 1994; 1997a; 1997b; Frank and Paterson, 2001). Attempts for understanding the characteristics and the dynamics of Iogenic particles inside the Jovian magnetosphere are not only driven by the interests in magnetospheric science, but also the Io tori directly associate with the Io's volcanic activities (e.g. Herbert et al., 2001; Mendillo et al., 2004, 2007; Nozawa et al., 2004; Yoneda et al., 2010; 2014). The recent developed technique of energetic neutral atom (ENA) imaging has the potential to provide information concerning the Io plasma and neutral tori in an efficient manner.

1.2 Energetic neutral atom imaging in Jovian system

ENA imaging is a technique for the remote investigation of the interaction between space plasma and neutrals (e.g. Roelof and Williams, 1988; Gruntmann, 1997). Several ENA instruments have been carried into space, and the data collected by these instruments have been used to study the interactions between space plasma and neutral gas (e.g. Burch, 2000, 2003; Krimigis et al., 2002; Mauk et al., 2003; Brandt et al., 2005; Futaana et al., 2011; Goldstein and McComas, 2013). More recently, ENA imaging has also been successfully applied to investigations of the interactions between space plasma and the Moon surface (e.g. Futaana et al., 2006; McComas et al., 2009; Wieser et al., 2009; Schaufelberger et al., 2011; Futaana et al., 2012).

ENAs near Jupiter were detected by the Voyager 1 low-energy charged particle (LECP) instrument. LECP is a sensor for high-energy plasma particles, (Krimigis et al., 1977) but Kirsch et al. (1981) concluded the energetic neutral atoms were a possible explanation of one of the observed signals. Cheng (1986) calculated the interaction between plasma and neutral atoms in the inner magnetosphere and concluded that the charge exchange makes a significant contribution to the fluxes of energetic neutral particles. Based on the dedicated ENA measurement performed by Cassini/INCA, Krimigis et al. (2002) reported the firm evidence of high-energy ENAs (HENAs; >10 keV) emitted from the Jupiter system. Later, Mauk et al. (2003) claimed that the observed ENAs in the range of 50–80 keV originated from a region slightly outside of the Europa orbit (trans-Europa gas tori).

These previous observations of ENAs in the Jupiter environment were only conducted in the high-energy regime (>10 keV). No low-energy ENA (LENA) instrument (with a typical energy range of 10 eV to a few keV) has been employed in the Jovian system, although there are some speculation for studying moon-plasma interactions [Plainaki et al., 2010; Mililo et al., 2013; Grasset et al., 2013]. This unexplored energy range of LENAs is expected to provide us with valuable information regarding the characteristics of the Io tori, their formation and loss mechanisms, and associated transport mechanisms of iogenic materials. Whereas a fraction of the energy is carried by high-energy particles in the Jovian system, the mass transfer, namely, the outward transport of iogenic materials, is dominated by low-energy particles (Bagenal and Delamere, 2011). From this perspective, the low-energy particles are essential to the characterization of the Jovian plasma environment.

1.3 Low-energy Energetic Neutral Atom imaging

Several LENA instruments have been used to investigate extraterrestrial environments. For example, the Neutral Particle Imager and Neutral Particle Detector were placed on board European Space Agency's (ESA's) Mars Express to establish a basic understanding of the ENA environment of Mars (Barabash et al., 2006). Replicas of these detectors were flown to Venus on the Venus Express mission (Barabash et al., 2007). IBEX-Lo has imaged the heliopause from the Earth orbit (McComas et al., 2009). The Chandrayaan-1 Energetic Neutrals Analyzer (CENA) was placed into Moon orbit (e.g., Kazama et al., 2006; Barabash et al., 2009), providing evidence of interaction between the solar wind and regolith surface. A replica of CENA, named Energetic Neutrals Analyzer (ENA), will be flown to Mercury with the ESA-JAXA joint mission, BepiColombo as a part of Mercury Plasma Particle Experiment (MPPE) on the Mercury Magnetospheric Orbiter (MMO) spacecraft (Saito et al., 2010). BepiColombo will also carry another LENA sensor, as part of the Search for Exospheric Refilling and Emitted Neutral Abundances (SERENA) package, on the Mercury Planetary Orbiter (MPO) spacecraft (Orsini et al., 2010). These aim to image Mercury-plasma interaction by LENAs (e.g. Grande 1997; Barabash et al., 2001; Orsini et al., 2001; Massetti et al., 2003).

In 2022, ESA will launch its first Jupiter mission, JUpiter ICy moons Explorer (JUICE; Grasset et al., 2013). JUICE is equipped with a complete plasma package, Particle Environment Package (PEP), which includes a LENA sensor named Jovian Neutrals Analyzer (JNA). The measurement principle of JNA is identical to that of ENA and CENA (Kazama et al., 2006; Barabash et al., 2009).

In this paper, we estimate the LENA flux produced by charge-exchange reactions between particles in the Io neutral and plasma tori to demonstrate the feasibility of LENA observations from Ganymede orbit using existing LENA sensors. We assume simple models of the plasma and neutral tori. There are several reasons for using the simple models; first, such models require only a relatively short computational time for iterative calculation of the densities and velocity distribution functions of plasma and neutral tori; second, the line-of-sight integration for the LENA calculation will obscure details of small structures in any case; and third, simple models provide morphologic pictures that are useful for examining the application of this new technique of the LENA imaging to unexplored environment. The model is static, although the Io plasma and neutral tori are known to have temporal variations (e.g. Frank and Paterson et al., 2001; Herbert et al., 2001; 2003; Delamere et al., 2004; Nozawa et al., 2004; Yoneda et al., 2009; Steffl et al., 2004a; 2006). This is because this paper aims to understand the characteristics of LENA flux, particularly its intrinsic variations of the LENA flux due to the measurement technique and its limitations. In section 4, environmental variations, which are important for understanding nature of the Io tori, will be discussed.

We calculate the LENA flux along the planned trajectory of the JUICE spacecraft (Grasset et al., 2013) and discuss the observation capabilities of JNA on board. In addition, we discuss the possible physics to be explored by JNA as well as the constraints for operating the sensor and analyzing the obtained dataset. We do not attempt to discuss the detailed physics of the Io tori in this paper.

2. Models

The primary generation mechanism of LENAs near the Io tori is charge-exchange (also called "charge transfer"). Because of the co-existence of ions and neutral atoms, ions in the plasma torus (X^{n+}), experience charge exchange with neutral atoms in the neutral torus (Y):

$$X^{n+} + Y \rightarrow X^{*} + Y^{n+}$$

After the charge exchange, a neutral atom (X^{*}; ENA) and an ion (Y^{n+}) are formed. The newly ionized particles begin to corotate. The newly born neutral atoms have nearly the same energy (e.g. Rees, 1989) as that of the primary ion, which corresponds to the corotational flow (~74 km/s at the Io orbit, or ~29 eV/amu, namely ~29 eV for H, ~460 eV for O, and ~920 eV for S). The energies of these atoms are in the LENA energy range.

To calculate the expected LENA flux, one must construct models of the plasma and neutral tori. In addition, the cross sections for the relevant charge-exchange reactions are required. From those models, we can derive the expected ENA fluxes using the following formulation.

$$f_{\mathrm{ENA}}(\vec{r_0}, \vec{v_0}; t=0) = \int_{-\infty}^{0} f_{\mathrm{plasma}}(\vec{r_1}, \vec{v_1}; t_1) \cdot \sigma \cdot N_n(\vec{r_1}, t1) dl$$

Here, f_{ENA} is the ENA flux at the spacecraft position $\vec{r}_0$ and with the velocity $\vec{v}_0$ at a certain time (*t*=0). The integral is taken from the spacecraft position back in time along the Kepler trajectory of the ENA. The distance along the trajectory is denoted by *l*. The plasma velocity distribution function f_{plasma} is calculated for the position $\vec{r}_1$ and velocity $\vec{v}_1$ at generation, which are also determined from the Keplerian motion. N_{n} is the neutral density, and σ is the charge-exchange cross section. Details of the formulation are described in Appendix A.

Several sophisticated neutral-torus models have been proposed, and some of them reflect the physics very precisely (e.g. Smyth, 1992; Wilson et al., 2002; Smyth and Marconi, 2003). However, based on a simplified approach, we constructed our neutral-torus model in an analytic form. We modeled the density as a sum of two exponential distributions:

$$n(R,\theta) = n_0 \exp\Big(-\frac{|\theta|}{\theta_0} - \frac{|R|}{R_0}\Big) + n_1 \exp\Big(-\frac{|\theta|}{\theta_1} - \frac{|R|}{R_1}\Big)$$

$$\theta_i = \begin{cases} \theta_{ih} & (\theta > 0) \\ \theta_{it} & (\theta < 0) \end{cases}$$

Here, $n(R, \theta)$ is the density at the distance R from the Io torus and the separation angle (θ) from the Jupiter-Io line and n_0 and n_1 is the number densities for each distribution. The parameters θ_0, θ_1, r_0, and r_1 define the spread of the distribution. Different θ_0 values are used to consider the asymmetry between the leading and trailing parts of the torus; namely, θ_{0h} is used for the leading part (θ>0), and θ_{0t} is used for the trailing part (θ<0). The assumed values are as follows: n_0 = 15000 cm^{-3}, R_0 = 0.072 Rj, θ_{0h} = 14.4°, θ_{0t} = 3.6°, n_1 = 50

cm^{-3}, $R_1 = 0.72$ Rj, $\theta_{0h} = 86.6°$, and $\theta_{0t} = 14.4°$. The typical density of the neutral torus on a global scale is controlled by the second component (parameter n_1). This value was selected to be very close to those used in previous studies, such as Johnson and Strobel (1982) and Cheng (1986). Figure 1b compares the results obtained using the simple model employed here and a numerical model proposed by Smyth and Marconi (2003). Parameters in our simple model was chosen to capture the general trend of the Io neutral torus. However, our model underestimates the neutral density in most of the region. In some region, the underestimation is by a factor of 10 or more. For our purpose of demonstrating the feasibility of LENA imaging from Ganymede orbit, an underestimation of the LENA flux is preferable rather than an overestimation. The neutral-torus model does not include any composition (H, O or S) information. Although the neutral composition only plays a key role to the amount of ENA via the cross section, the composition information will be reflected into only the cross section model. All neutral atoms are assumed to move at a speed that corresponds to Io's orbital velocity.

For our plasma-torus model, the same argument for using a simple analytical model is applied. In practice, the simplicity is of great benefit with respect to the impact on computational resources because we need to calculate the velocity distribution function of ions in the plasma torus (Appendix A). We assumed the following model. The plasma-torus structure is independent of the Io phase. Although there are a few models that better represent the Jovian magnetosphere (e.g., Acuña and Ness, 1976; Dougherty et al., 1996; Connerney et al., 1998), we employed a perfect dipole here. We used the dipole component parameters from the O4 model, namely, the tilt of the dipole field is 9.6°, pointing to the west longitude of 201.7° in the System III coordinate system (Acuña and Ness, 1976). However, it is known that the central plane (peak density along a magnetic field line) of the plasma torus is located at the centrifugal equator (Hill, 1974; Bagenal and Sullivan, 1981), which is between the Jovian equator plane and magnetic equator plane. The maximum separation between the centrifugal equator and magnetic equator is ~3.2° (Hill, 1974). Therefore, we assumed the tilt of dipole axis to be 6.4° to emulate the centrifugal equator instead of using the actual tilt of ~9.6° above. Indeed, the change in the tilt angle of the dipole axis does not impact on the morphologic views of the following results.

The total density of plasma-torus ions at the magnetic equator, n_L(r), was taken from Divine and Garrett (1983) but slightly simplified inside the Io distance (Figure 2b). Figure 2b also indicate values of other existing models: Bagenal (1994), based on Voyager 1 data later validated by Galileo data; and Bagenal and Delamere (2011) based on Galileo data. These models provide slightly higher values especially in the inner region, but anyway, less than a factor of 10 of the present model. Away from the equator, we modified the density by the scale height of H, $\exp(-z/H)^2$, adopting Hill and Michel (1976) and other authors (e.g. Bagenal et al., 1994; Bagenal and Delamere, 2011). Here, z is the distance from the centrifugal equator along the field line and H (Rj) is $0.64\times(Ti(eV)/Ai(amu))^{1/2}$. We assumed the bulk plasma to flow azimuthally with the corotation velocity and the thermal speed, v_{th}, corresponding to 70 eV for all species (Kivelson et al., 2004). For O^+, this value corresponds to v_{th} ~5.5 km/s. The assumed temperature of 70 eV is slightly higher than the data obtained from Voyager 1 PLS and Galileo PLS by a factor of 2–3 (see Figure 3 in Beganel and Delamere, 2011), while the difference in thermal velocity is less significant (√2–√3). We assume that the velocity distribution function is an isotropic Maxwellian. This assumption significantly underestimates the high-energy portion of the velocity distribution.

We also require cross-section models for the charge-exchange reactions. There are three main neutral components (S, O, H, and their compounds) and their ions (S^{n+}, O^{n+}, and H^+). Table 1 provides a list of the expected charge-exchange cross sections (Johnson and Strobel, 1982; McGrath and Johnson, 1989) for a relative velocity of ~60 km/s. The typical cross section for charge exchange is ~(1–50) x 10^{-16} cm^2 in this energy range. Rather large deviations in cross-section values have been reported in some cases. In such cases, we use the lowest quantities, resulting in an underestimation of the LENA production. We consider only the charge exchange reactions that produce LENAs directly. For example, the reaction $O^{++} + S \rightarrow O^* + S^{++}$ is considered between doubly charged ions (for example O^{++}) and neutrals (e.g. S). There are of course the reaction of single electron transfer, namely, $O^{++} + S \rightarrow O^{+} + S^{+}$. However, since this reaction does not produce LENAs directly, we should not consider it.

To simplify the calculation, we calculated the total cross section as defined below. First, we take the average of cross section for each parent ion species, weighted by the fraction of neutral composition. This is the "convolved cross section" in Table 1. This convolved cross section is the single value but equivalent to the cross section of a parent ion for charge exchange process through the multiple-species Io neutral torus. Here, the average relative composition of S and O near the neutral torus is 1:4 (e.g., Johnson and Strobel, 1982). The H population is assumed to be 10% of the total assuming stoichiometry. We neglect the molecular contributions to the cross-section calculations, primarily because we could not find good reference data to constrain the fraction and the charge exchange cross sections. Then, we again take the weighted average to obtain the total cross section for each LENA species, considering the parent ion’s charge state. This is the cross section for charge exchange production for specific LENA species from different charge-state parent ions. The total calculated cross sections are 12, 19, and 9 x 10^{-16} cm^2 for H, O, and S, respectively (Table 1).

After calculating the LENA flux, we further evaluated if a conventional LENA sensor can measure the Io torus image. As a reference instrument used in this paper to calculate the LENA count rate to evaluate the measurement feasibility, we consider the current design of the JNA instrument (hereafter referred to as the JNA-prototype) prepared for the JUICE spacecraft. The JNA-prototype has similar capabilities to the MPPE/ENA sensor and Chandrayaan-1/CENA sensor (Kazama et al., 2006; Barabash et al., 2009). See Table 2 for a summary of the specifications of the JNA-prototype.

3. Model Results

3.1 Io-torus LENA flux

Figure 3 presents an image of simulated differential flux of the LENAs emitted from the Io tori. The oxygen and sulfur LENA images for the energy of 210 eV and 420 eV (both for ~50 km/s) is displayed as examples. The observer is placed at the planned location of the JUICE spacecraft during its so-called high-latitude imaging period (Grasset et al., 2013). During this period, the spacecraft will have a slight inclination with respect to the equatorial plane. We show here the case when the spacecraft was located at 23.3 Rj at the latitude of 6.5° north from the Jovian equatorial plane.

The peak flux can reach 10^5 /cm^2 s eV sr in this case. The shape of the LENA image is similar to a slice of the Io plasma torus. The image exhibits a very narrow angular distribution. One can see a shift in the peak signal toward Jupiter by ~10°. This shift is caused by the spacecraft velocity effect (aberration). The simulated image clearly illustrates that the contribution of the spacecraft motion cannot be neglected. The spacecraft is typically moving at 10 km/s, and thus, the aberration effect is, at maximum, ~10° for 50 km/s LENAs when the ENA flow direction and the spacecraft velocity vector is perpendicular. When they are parallel, this effect can be seen as a change in the observed ENA velocity. The spacecraft velocity effect can be corrected by subtracting the velocity of the spacecraft from the image in the actual data analysis (Appendix A). Figure 3 also displays a strong signal from the "left" side of Jupiter in the figure, where the north of Jupiter is drawn to be up. On this side, the Io tori particles move toward the observer so that the generated ENAs fly to the spacecraft. Although the corotation plasma undergoes charge exchange when Io is located on the other side ("right" side in Figure 3) of Jupiter, the generated LENAs will travel away from the spacecraft. Therefore, the instantaneous image has a strong asymmetry. In the followings, we refer to the "left" side (strong LENA flux) as toward side and the other as away side. The degree of toward-away asymmetry depends on the temperature of the corotating plasma. More asymmetry is expected for cooler plasma.

Figure 4 presents a series of LENA images taken along the planned orbit of the JUICE spacecraft. Oxygen ENA images with the energy of 210 eV, same condition as Figure 3, are shown as examples. The corresponding locations of the spacecraft are marked at the center of the figure. The LENAs from the Io tori are always seen from the toward side of Jupiter regardless of the relative position of the observer with respect to Jupiter and Io. The peak flux varies from 10^3 to 10^5 /cm^2 s sr eV. In contrast, the intensity clearly depends on the relative position. We can detect a strong flux from the Io tori when the LENAs that are generated from the side with the corotating plasma move toward the spacecraft (equivalently, when Io is located on the toward side of Jupiter). The highest flux is obtained at Jupiter-Io-Observer angle of ~165˚ in this case (18 UT on May 20, 2031). This time is ~8 hours after the Jupiter-Io-Observer angle is 90˚ (at 10 UT on May 20, 2031), when the maximum flux would be expected from the naïve prediction. This apparent discrepancy can be simply explained once we consider the flight time of the LENAs. Even if the maximum flux is produced when the Jupiter-Io-Observer angle is 90˚, the LENAs take a few hours to reach to the spacecraft. For oxygen LENAs with a speed of ~50 km/s, traversing the distance of over 15 Rj (~10^6 km) from Io to the spacecraft takes 2×10^4 s (~6 h). As one might expect, the time lag depends on the velocity of the LENAs.

The time series of the LENA count rate to be observed by the JNA instrument (Table 2) at the JUICE location is shown in Figure 5. The spacecraft is assumed to point toward Jupiter, and the right edge of the aperture is aligned with Jupiter (gray dotted rectangle in Figure 3). The count rates of three species (H, O, and S) are calculated by integrating the simulated LENA flux over the sensor pixel shown in Figure 3. The calculated peak count rate is 1-100 counts per second for all species. The O flux is most prominent because O is the dominant species in the plasma torus. The mass-dependent bulk energy of each species corresponds to the corotation velocity. Note that the peak energy appears to be higher than the corotational energy in Figure 4; this is mainly because the count rate is proportional, provided the g-factor is constant over the energy, to the energy flux, not the particle flux, so that the peak count rate shifts toward the higher energy.

The spectrogram displays several characteristic features. First, there is a clear ~10 h periodicity. This periodicity arises from the rotation of the Jupiter's magnetosphere. The neutral torus moves up and down with respect to the plasma-torus structure, and the number of charge-exchange reactions varies accordingly, peaking when the magnetic equator is in line with the Io neutral torus. Second, there is a ~50 h periodicity. This periodicity is associated with the rotation of Io (and the resulting Io neutral torus) around Jupiter with a period of ~42.5 h. Precisely speaking, this periodic feature is the synodic period of Io and the spacecraft. We can also observe the dispersion-like signatures because of the flight time of the LENAs from the torus to the spacecraft, which depends on their velocity. A lower LENA energy will cause the LENA to take longer to reach the spacecraft. The time scale of the dispersion is several hours.

3.2 Loss of LENAs

After being generated near the Io tori, some LENAs may be lost before arriving at the spacecraft. Thus, we must evaluate the importance of the loss processes. Here, three loss mechanisms are considered: electron impact ionization, charge exchange, and photoionization.

The probability of electron impact ionization p_{ei} is estimated as follows:

$$p_{\mathrm{ei}} = \int_0^\infty n_e(l)\sigma_{\mathrm{ei}}(E)dl \sim \langle n_e \rangle \sigma_{\mathrm{ei}} L$$

where n_e and $<n_e>$ are the electron density and its average along the trajectory, respectively; l is the distance along the trajectory; σ_{ei} is the electron impact ionization cross section, which is a function of the impact energy; and L is the typical scale length.

To determine the upper limit, let us consider the maximum cross section σ_{ei} = 1.5x10^{-16} cm^2 (for ~100 eV electrons; Kim and Desclaux, 2002) and the maximum electron density ~2000 cm^{-3} (near Io; Kivelson et al., 2004) over the traveling length of L = 15 Rj (~10^{11} cm). The resultant calculated probability of electron impact ionization is $p_{ei}=<n_e>\cdot \sigma_{ei} \cdot L=3\times10^{-2}$. This value includes a large margin for error, and in reality, the loss probability must be considerably smaller. The electron temperature is ~10 eV at Io's orbit (Kivelson et al., 2004), which is smaller than the oxygen ionization potential. In this case, the cross section for ionization is negligible. The electron temperature reaches a few 100 eV near Europa or Ganymede, while in these regions, the electron density is one to two orders of magnitude smaller than the assumed density. The high-energy tail (including radiation-belt energy) of the electrons contributes to the ionization, but the cross section is again much smaller (e.g. Itikawa and Ichimura, 1990).

The generated LENAs can also experience charge exchange once again with other ions, thereby becoming re-ionized. The generated ions begin corotating around Jupiter, and the generated neutral atoms should be considered as ENAs, but their velocities become consistent with the local corotational speed. A similar calculation can be performed as for electron impact ionization, and the probability of charge exchange is

$$p_{\mathrm{cx}} = \int_0^\infty n(l)\sigma_{\mathrm{cx}} dl \sim \langle n \rangle \sigma_{\mathrm{cx}} L$$

The density, <*n*>, is the density of the plasma and takes a maximum value of 2000 cm^{-3}; σ_{cx} can reach as high as 10^{-15} cm^2. If the distance L is taken along the whole travelling length of 15 Rj (~10^{11} cm), the loss fraction calculated using these values is 0.2. Again, the obtained value is an upper limit with a large margin for error, particularly because of the plasma and neutral densities quickly decreases from the Io orbit. Plasma density drops by one order beyond 2 Rj (Figure 2b). The neutral density drops much quicker (Figure 1). Therefore, the loss fraction should be much lower in reality, more than by one order (<<0.02).

Photoionization is another potential loss process. The ionization potentials for the relevant species are ~10 V (10.4 V for S and 13.6 V for O and H), and thus, the impinging photons should have energies of more than 10 eV (wave length <100 nm; V-UV, E-UV and shorter). The only possible source of such short-wavelength photons is the Sun. At the typical solar irradiance, the power in this wavelength range is rather constant at 10^{-4} W m^{-2} nm^{-1} at 1 AU (e.g., Schmidtke et al., 2006). Thus, the total photon flux can then be estimated to be ~3×10^8 cm^{-2} s^{-1}, and at the Jupiter orbit (~5.9 AU), it is reduced to ~10^7 cm^{-2} s^{-1} integrated over wavelengths of <100 nm. The cross section of the photoionization reaches a maximum of ~2×10^{-17} cm^2 at 65–70 nm for oxygen atoms, according to the EUVAC model (Richards et al., 1994). To obtain an upper limit, we simply take the peak value over the entire wavelength range, which yields a loss rate of ~2×10^{-10} s^{-1}, and thus, the minimum LENA lifetime is estimated to be 5×10^{9} s. This lifetime is sufficiently long compared with the flight time of LENAs (10^{4}–10^{5} s) that we can neglect the loss caused by photoionization.

In conclusion, ENA loss between the Io tori and the observer is not very large, and thus is not critical for Io-tori LENA imaging. Indeed, because the energy range of interest in this work is rather restricted, the energy dependence of all loss mechanisms is weak so the shape of the energy spectrum is conserved. Thus, losses of LENAs do not significantly impact the feasibility of LENA imaging and associated scientific achievements.

3.3 Sensor capabilities

The expected differential flux is typically ~10^{3}–10^{5} cm^{-2} s^{-1} sr^{-1} eV^{-1} (Figures 3 and 4) at the Ganymede distance. This flux corresponds to ~1–100 counts per second by considering the JNA-prototype performance at the JUICE planned orbit (Figure 5). However, one difficulty of collecting instantaneous observations of Io torus ENA from the Ganymede distance is that Io LENAs have a narrow angular beam-like structure with a full width half maximum of <5°, which is rather small in comparison with the JNA-prototype angular resolution of ~30x5°. Thus, fine structures may be hidden in one angular pixel. Better angular resolution is required to resolve these fine structures. Although the peak count rate is enough in the detectable level, a longer integration time may be beneficial for investigating the energy spectrum or the spatial distributions. For example, a change in the global morphology of LENA specta, such as the dispersion relations seen in Figure 5, can be identified even when integrating over several to tens of minutes. Let us suppose here a 10-min integration (during which the spatial configuration would not change significantly) with 8 energy steps, then ~75 s integration is possible for each energy step, and the corresponding number of counts will be increased to 75–7500 counts. Indeed, a longer time integration will also aid in decreasing the telemetry and in reducing the ambiguity of background counts that originate from the intense Jovian radiation environment.

4. Scientific objectives

In this section, we discuss what information can be obtained from LENA measurements of the Io tori and what scientific objectives we can address using these data. Table 3 summarizes the quantities that LENA data can (and cannot) provide. Detailed explanations and justifications are discussed in the following.

4.1 Io-tori characterization

LENA data can provide physical quantities that describe the plasma torus. The shape of the energy spectrum of the LENAs and their chemical (mass) composition can be obtained. The energy spectra directly reflect those of the Io torus plasma, thereby, providing information that is critical to understanding the characteristics and dynamics of the plasma in the plasma torus. The velocity of the plasma in the torus and its temperature can also be calculated using the LENA measurement. The absolute densities of the neutral and plasma tori cannot be easily deconvolved from the LENA dataset alone because the LENA data provide only a line-of-sight integral of a convolution of both densities.

The mass information reflects the chemical composition in the plasma torus. The mass composition is strongly influenced by generation and loss mechanisms (e.g. Frank and Paterson, 2001; Delamere et al., 2004; Hansen et al., 2005; Steffl et al., 2006). For example, if the O^+/S^+ ratio is two, one may infer, under the stoichiometric assumption, that the Io plasma torus originates from volcanic Io materials (SO_2) and that the loss mechanism does not depend on species. Deriving the mass fraction of H^+ will aid in understanding the dynamics of protons in the Jovian magnetosphere. Proton distribution in the Io torus is not a well constrained information (e.g. Thomas et al. 2004). Although the proton fraction has been assumed 10%, there are several measurements showing much smaller fraction than 10% (e.g. Wang et al., 1998a, b; Zarka et al., 2001). The discrepancies indicate strong spatial or temporal variations. LENA imaging can reveal proton fraction and its spatial distribution instantaneously.

The charge state of ions in the plasma torus, e.g., S^+ and S^{++}, might be derived from the different shapes of the energy spectra. Because of the M/q difference between different charge states, different charge-state ions of the same species can have different energy spectra (e.g., temperatures). For example, S^{++} (M/q = 16) is expected to have a temperature similar to O^+ (M/q = 16) but different from S^+ (M/q = 32), if one attributes the ion temperatures in the plasma torus to the pickup process. It is also believed that the Io plasma torus is not in chemical equilibrium (e.g., Thomas et al., 2004), implying that there is no reason that S^+ and S^{++} should have the same spectral shape. The separation of charge states using the LENA velocity distribution functions may be a realistic goal.

Whereas the LENA energy spectra and LENA mass spectra reflect the plasma-torus characteristics well, the neutral-torus characteristics are more difficult to obtain. In theory, the velocity of the neutrals in the torus and the mass composition are convoluted in the cross section. However, to extract this information from the actual data is quite difficult. There is an uncertainty in the velocity dependence of the cross section. The charge-exchange cross sections associated with S are particularly difficult to obtain in laboratory measurements, as S tends to react chemically with ambient gas and instrumentation. Thus, we must refer to theoretical calculations (e.g. Johnson and Strobel, 1982). Other complimented observations (Section 5.2) or modelling effort to restrict the LENA data interpretation (Section 5.2) would be more realistic way of investigation.

4.2 Short-term variations

Short-term temporal variations (or, in particular, abrupt variations) in the plasma and neutral tori, if they occur, can result in corresponding variations in the LENA flux. From continuous time series of LENA energy and mass spectra, one can identify which of the tori is responsible for the LENA variation. This separation can be achieved because of the different responses of the LENA flux to the changes in the plasma and neutral tori. When the density of the neutral torus increases abruptly for some reason, the LENA flux increases regardless of energy and mass; more precisely speaking, the change would be proportional the cross sections to the relative, but it can be distinguished. In contrast, there is a high likelihood that a temporal variation in the plasma torus would induce modifications only at specific energies and/or masses. For example, in the case of sporadic injection of plasma into the plasma torus, the LENA image would be affected only at the corresponding energy and/or mass of the injection.

Another possible phenomenon for investigation is the hypothetical O and S streams. Na is known to exhibit a short temporal scale (<10 hours) and relatively small spatial scale (a few Io radii) stream (e.g., Schneider et al., 1991; Wilson et al., 2002; Thomas et al., 2004; Schneider and Bagenal 2007). Although the existence of similar streams for O and S is thought to be less plausible because of the different characteristics (timescales and chemical reactions) of Na, O, and S, LENA imaging may provide information to place limit on the existence of fast O and S stream in the near Io environment.

4.3 Long-term variations

From Galileo observations, the plasma-torus density is known to vary significantly over time. Frank and Paterson (2001) claimed that the density of the Io plasma torus during the 1995 flyby was three to four times higher than during the other flybys in 1999 and 2000. One of the hypothetical sources of enhancement of the Io tori is variable volcanic activity. Indeed, the UV measurement performed by Cassini indicates a long-term (week to month) change in the tori, which may be attributed to volcanic activity (Schneider and Bagenal, 2007). Ground-based observations indicate systematic long-term correlations between the volcanic activities and the emission of IR (Nozawa et al., 2004; Yoneda et al., 2010).

If volcanic activities increase, the neutral-torus density initially increases. After a period of time (the ionization time scale depends on the mechanisms, being typically a few hours; e.g., Smyth and Combi, 1988; Schneider and Bagenal., 2007), the higher-density neutrals become ionized to form a denser plasma torus. The higher density plasma torus may retain more than 10s of days (e.g. Schneider and Bagenal, 2007). We can monitor the evolution of the Io tori by tracking these temporal changes; first ENA flux increases almost independent of the species and energies because of the increase of neutral component, followed by species-by-species energy dependent increase due to the increase of the plasma composition, depending on the generation and loss mechanisms.

4.4 Transport

ENAs are considered to be one of the transport mechanisms of materials from the Io orbit outward. Because of Io's volcanic activity ~10^{28} particles are introduced into the neutral torus per second, and (1-2)x10^{26} ions are transported out of the Jovian system per second via the charge-exchanged ENAs in the high-energy domain of the Cassini/INCA sensor (Krimigis et al., 2002). These authors also inferred that the total escape flux, including lower energies, is 10^{27}/s, which is 10% of the generated flux. The direct measurement of the LENAs will provide a more precise estimate of the loss rate from the torus via the charge exchange.

Figure 6 shows the LENA distribution seen on the global scale of the Jovian magnetosphere. Each dot corresponds to a LENA, which are emitted from Io tori with the velocity of the corotation and a thermal spread of 5.5 km/s (T~70 eV for O is assumed). The global LENA distribution forms a spiral shape, although each LENA is traveling almost radially. This spiral shape is conceptually similar to the Parker spiral of the solar wind magnetic field or water ejected from a rotating sprinkler. To produce this plot, we did not consider the Jovian magnetic field tilt for simplicity. Inclusion of the tilt will embed a ~10 hour modulation (corresponding to ~85° in the azimuthal direction).

The transfer from Io is not axisymmetric inside the Jovian magnetosphere. If one is located at a certain point, the LENA flux from the Io torus is measured as an intermittent flow. In contrast, the thermal spread of the Io plasma and distribution of the generation point (although it is close to Io position) will dissipate the shape of the spatial distribution in the very far tail (>~150 Rj with the parameters used in this calculation). This image can be complemented by the "neutral nebula" concept formulated by Krimigis et al. (2002), in which they suggested a disk-like confinement of LENAs in the Jovian equatorial plane generated by Io's (or other moons') tori. However, the view provided in Figure 6 indicates a spiral structure inside the nebula.

4.5 Lag of the plasma corotation

Based on Voyager 1 plasma sensor data, McNutt et al. (1979) reported that the Jovian magnetosphere exhibits a slightly slower than "perfectly" rigid corotational flow. This velocity lag has been identified even at Io's distance. The in situ plasma measurements collected by Galileo indicated that the lag is ~2–10 km/s, with an average lag of 2–3 km/s (Frank and Paterson, 2001). Higher velocities than the corotational velocity have never been observed. Hill (1980) suggested that the lag is the effect of mass loading. Another suggested mechanism is the hypothetical latitudinal differential rotation of the Jovian magnetosphere (Dessler 1985). Long-term observations permitting the characterization of the velocity of the plasma torus can restrict the possible slow-down mechanisms of the plasma torus in the vicinity of Io. If we can point the FOV of JNA perpendicular to the magnetic equatorial plane (perpendicular to the pixel shown in Figure 3), the collected LENA data along the FoV will provide the latitudinal difference in the torus velocity. This operation will test the differential-rotation hypothesis. By investigating the correlations between the torus densities and the velocity lag determined from LENA measurements, one may also constrain the momentum transfers between the plasma and neutral tori, which directly contribute to the mass loading.

The typical velocity lag is 2–3 km/s, which corresponds to ~3–4% of the corotational velocity (and to ~5-8 % of the energy). Distinguishing an energy difference of <10% from JNA data may not be a straightforward analysis, but it should still be possible if one employs proper analysis methods. For example, as in Futaana et al. (2013), it is possible to clearly distinguish the LENA flux for parametric temperatures of ~85 eV from that for 75 eV (a ~10% difference in energy). When the velocity lag is as large as 5–10 km/s (~7–13% of the corotational flow), the energy difference becomes ~15–25%, and the possibility of the discrimination becomes more promising.

5. Operation, Collaboration, and Data analysis

5.1 Challenges

Although a sufficient count rate of LENAs from the Io tori is expected, operating the LENA instrument during the real mission and analyzing the obtained data pose a considerable challenge. The limited field of view (FOV) is the most problematic issue. The FOV of the existing LENA sensors is a single-pixel camera (McComas et al., 2009) or a fan-shaped 1-D aperture (Barabash et al., 2009), and thus, the angular acceptance is very small. When this small acceptance is combined with the relatively small angular spread of the Io-torus LENA image, a small shift in the aperture results in the loss of the LENA signal peak. Although we may know the predicted attitude of the spacecraft beforehand in the practical operation, pointing toward the Io torus is not a simple task. The spacecraft velocity (ram velocity) is not negligible for Io-torus LENA imaging (Figures 3 and 4), and the optimal compensating angle depends on the energy of LENAs. Thus, there is no unique optimal solution for spacecraft pointing that captures the maximum fluxes for all energies. A rather good argument here is that the data analysis after data reception is simpler because all information necessary to correct the aberration effect is known.

The second problem is the LENA flight time. The typical measurement of the Io torus by the JUICE spacecraft will be performed at the Ganymede orbit (~15 Rj) or farther. For the LENA with a velocity of 74 km/s, the flight time is ~1.4×10^4 s. Because Io rotates around Jupiter in ~42.5 h, Io moves more than 30° in the time it takes for the LENAs to reach the instrument. For the instrumental operation, we should refer not to the Io's position at the operating time but the position several hours before depending on the LENA energy. As shown in Figure 4, we can clearly see a peak emission a few hours after the apparent optimal condition.

Third, the gravitational force exerted by Jupiter affects the LENA trajectories and causes them to become to ballistic trajectories. The degree of bending depends on the velocity, but the low-velocity LENAs are most strongly affected. The gravitation force is a well-known parameter, and its influence is smaller than that of the flight time discussed above; however, the gravity force must be properly considered for precise analysis of the obtained data.

Fourth, the charge-exchange cross sections are still not well constrained. They also depend on the relative velocities between the plasma and neutral particles in the tori. However, the dependency is not very strong within the LENA energy range. For example, for the O^+–O interaction, the variation with energy is approximately a factor of two to three between 40 eV and 10 keV (Lindsay and Stebbings, 2005). Nevertheless, when one calculates the physical quantities of the tori (e.g., the density, composition, and other quantities) from the obtained data, the uncertainty of the cross sections directly impacts the uncertainties of those quantities.

5.2 Synergy with Other Measurements

HENAs are also expected from high-energy particles in the plasma torus. JNA will be accompanied by the Jovian Energetic Neutrals and Ions (JENI) sensor, which is also included as a part of the PEP suite to detect HENAs. Their energy range is planned to cover 0.5–300 keV. HENAs will be detected even when fewer LENAs are detected (when Io is on the away side) because of the high thermal velocity of the original ions. HENAs provide information regarding characteristics of the Io torus plasma and Io's radiation environment, and moreover, they may preserve information concerning acceleration mechanisms. Thus, the combination of LENA and HENA time-series data will permit the investigation of the evolution of the acceleration of plasma in the plasma torus. In addition, JENI is capable of 2-D imaging. The simultaneous JENI imaging will extend the observable velocity and mass space of ENAs.

Another related science target to be investigated via the synergy between LENA and HENA data is the trans-Europa gas tori (Mauk et al., 2003). Based on a HENA (50–80 keV) image obtained using the Cassini/INCA instrument, the existence of Europa gas tori (composed of H and O) has been suggested, although this instrument has found no evidence of distinct Io-tori related HENAs. The corotational velocity at the Europa orbit is ~150 km/s, and thus, the core component (H and O) of ENAs generated in the Europa-tori also falls into the LENA energy range. Sulfur may reach ~4 keV, which is almost the upper limit of the JNA sensor. A LENA measurement will provide complimentary evidence of the existence of trans-Europa gas tori. Distinguishing between the Io and Europa tori from LENA data alone will not be simple because the JNA-prototype has a rather coarse angular resolution (Table 2). However, it will still be possible to distinguish between the Io and Europa tori using the energy spectra and their periodic features, the dispersion signatures and the mass spectra. The energy spectrum of LENAs from Io should have a peak at ~74 km/s, whereas the LENAs from Europa should have a peak at ~150 km/s, corresponding to their respective corotation velocities. In addition, the periodicity of the ENA signals, as seen in Figure 5, must differ according to the moons' rotation period.

LENA imaging can be compared with observations of UV emission to gain further understanding of the Io tori. The UV and LENA measurements are both imaging, so that the obtained data can be used complimentarily. A difference of characteristics is the LENA line-of-sight (trjaectory) is twisted by the gravity of Jupiter; therefore the different slice of of the information may be obtained. If the neutral (plasma) density is derived via the UV spectroscopy, the plasma (neutral) density can be derived using a LENA sensor, in principle. Another difference is the emission signature. Since the photon is emitted isotropically, the obtained image will be fundamentally different from the highly directional emission of LENAs. For example, the Io-torus UV emission measured using the EUVE satellite exhibits a dawn-dusk asymmetry, in which the dusk side is stronger, and there is no apparent Io-phase dependence (Gladstone and Hall, 1998). In contrast, the Voyager UV measurement did indicate an Io-phase dependence (Sandel and Broadfoot, 1982). These features in the UV images differ from the predicted LENA images, which exhibit a clear toward-away asymmetry in which the toward side is stronger. Although the toward-dusk asymmetry of the Io tori is essential to understanding the generation and loss mechanisms and the dynamics of particles in the tori, placing constraints on the asymmetry using the LENA dataset is a difficult task because the peak flux of the LENAs on the away side will never reach the spacecraft (because of the strongly directional flow of LENAs). This indicates that the LENA imaging have a information gap depending on the Io position: Recurrence of the measurement is ~50 hour for LENAs, so that any changes below the time scale in LENA signatures are hardly attributed to either the change in the neutral or the plasma tori. UV imaging will help to fill the gap of this information. Indeed, variations in such time scales have been reported. Many authors (e.g. Sandel and Dessler, 1988; Brown 1995; Frank and Petersen, 2001; Nozawa et al., 2004; Steffl et al., 2006) argued that a typical variation in tori characteristic period could be modulated by the so-called System IV period (~10.2 hours). Cassin UV spectroscopy reported the enhancement of the torus emission power by 20% for about 20 hours (Steffl et al., 2004). Such phenomena in these time scales are difficult to investigate only from LENA imaging.

Synergy with state-of-the-art data-analysis algorithms should also be mentioned here. The JNA-prototype provides angular separation in only one direction of the angle, which will limit the intuitive understanding of the LENA signal. We may require the aid of numerical models and/or inversion techniques. Such inversion techniques have been applied beginning with the early ENA observations (e.g., Demajistre et al., 2004; Galli et al., 2008a; 2008d; Nakano et al., 2008). Similar techniques should be optimized for each scientific objective, implemented and validated for interpreting LENAs that originate from the Io tori, considering all the affecting parameters (spacecraft velocity, flight time, and gravity).

5.3 Impact on spacecraft and mission design

One benefit of LENAs compared with in situ measurements is that LENAs can enable the remote sensing of particles in the Io tori. Without actually entering to Io’s orbit, we can investigate the near-Io neutral and plasma environment. A harsher will make the spacecraft and instrument designs more challenging. In addition, the background caused by radiation cannot be avoided, so one requires multiple-coincidence detection systems or longer time integrals to improve the signal-to-noise ratio for an in situ plasma sensor. These approaches typically lower the instrument sensitivity by a factor of 10–100.

6. Summary

We have calculated the flux and expected count rate of energetic neutral atoms in the low-energy domain (LENA) from the Io plasma and neutral tori. The expected total flux is 10^3–10^5 cm^{-2} s^{-1} sr^{-1} eV^{-1}, if one measures from the Ganymede orbit. The flux is comparable to or above the one-count-per-second level of the LENA sensor that has been designed for Jupiter exploration.

The time scale of the variation in the global morphology of the LENA flux is the rotation time of the Jupiter magnetosphere, which is ~10 h. A longer time scale of ~50 h, which corresponds to the synodic period of Io and the spacecraft, is also expected. Because of the flight time of LENAs, the LENA energy spectrum exhibits dispersion signatures, typically with a time scale of several hours. The angular spread is rather confined, and thus, the LENA sensor should be improved to achieve higher angular resolution for resolving fine structures.

In 2030, the Jupiter exploration mission JUICE will conduct the first Jovian LENA measurement using a LENA instrument, JNA. From LENA observations, we can derive the characteristic quantities such as the energy spectra, density, velocity, and the composition of plasma-torus particles. We can further investigate the temporal variations (both short- and long-term) of the tori, the transport of materials, and acceleration mechanisms.

Acknowledgments

The authors appreciate the development and provision of the cross-section database (http://physics.nist.gov/PhysRefData/Ionization/Xsection.html) operated by the National Institute of Standards and Technology (NIST).

Reference

Acuña, M. H., and N. Ness, The main magnetic field of Jupiter, *J. Geophys. Res.*, *81* (16), 2917–2922, doi:10.1029/JA081i016p02917, 1976.

Bagenal, F., and J. D. Sullivan, Direct plasma measurements in the Io torus and inner magnetosphere of Jupiter, *J. Geophys. Res.*, *86* (A10), 8447–8466, doi:10.1029/JA086iA10p08447, 1981.

Bagenal, F., Empirical model of the Io plasma torus: Voyager measurements, *J. Geophys. Res., 99*, 11,043–11,062, doi:10.1029/93JA02908, 1994.

Bagenal, F., The ionization source near Io from Galileo wake data, *Geophys. Res. Lett., 24* (17), 2111–2114, doi:10.1029/97GL02052, 1997a.

Bagenal, F., F. J. Crary, A. I. F. Stewart, N. M. Schneider, D. A. Gurnett, W. S. Kurth, L. A. Frank, and W. R. Paterson, Galileo measurements of plasma density in the Io torus, *Geophys. Res. Lett., 24*(17), 2119–2122, doi:10.1029/97GL01254, 1997b.

Bagenal, F., and P. A. Delamere, Flow of mass and energy in the magnetospheres of Jupiter and Saturn, *J. Geophys. Res., 116*, A05209, doi:10.1029/2010JA016294, 2011.

Barabash, S., A. V. Lukyanov, P. C. Brandt, and R. Lundin, Energetic neutral atom imaging of Mercury's magnetosphere 3: Simulated images and insrtument requirements, *Planet. Space Sci., 49*, 1685–1692, 2001.Barabash, S., et al., The Analyzer of Space Plasmas and Energetic Atoms (ASPERA-3) for the Mars Express mission, *Space Sci. Rev., 126* (1), 113–164, 2006.

Barabash, S., et al., The Analyser of Space Plasmas and Energetic Atoms (ASPERA-4) for the Venus Express mission, *Planet. Space Sci., 55* (12), 1772–1792, doi:10.1016/j.pss.2007.01.014, 2007.

Barabash, S., et al., Investigation of the solar wind-Moon interaction on board Chandrayaan-1 mission with the SARA experiment, *Current Science, 96* (4), 526–532, 2009.

Brandt, P. C., D. G. Mitchell, E. C. Roelof, S. M. Krimigis, C. P. Paranicas, B. H. Mauk, J. Saur, and R. DeMajistre, ENA imaging: seeing the invisible, *Johns Hopkins APL technical digest, 26* (2), 143, 2005.

Brown, R. A., Optical line emission from Io, in *Exploration of the Planetary System*, edited by R. A. Brown, pp. 527–531, Reidel, 1974.

Brown, M. E., Periodicities in the Io plasma torus, J. Geophys. Res., 100, 21,683–21,695, 1995.

Burch, J. L., IMAGE mission overview, *Space Sci. Rev., 91* (1-2), 1–14, doi:10.1023/A:1005245323115, 2000.

Burch, J., The first two years of Image, *Space Sci. Rev., 109*, 1–24, doi:10.1023/B:SPAC.0000007510.32068.68, 2003.

Cheng, A. F., Energetic neutral particles from Jupiter and Saturn, *J. Geophys. Res.*, *91* (A4), 4524–4530, doi:10.1029/JA091iA04p04524, 1986.

Connerney, J. E. P., M. H. Acuña, N. F. Ness, and T. Satoh, New models of Jupiter's magnetic field constrained by the Io flux tube footprint, *J. Geophys. Res.*, *103* (A6), 11,929–11,939, doi:10.1029/97JA03726, 1998.

Delamere, P. A., A. Steffl, and F. Bagenal, Modeling temporal variability of plasma conditions in the Io torus during the Cassini era, *J. Geophys. Res.*, *109*, A10216, doi: 10.1029/2003JA010354, 2004.

DeMajistre, R., E. C. Roelof, P. C. Brandt, and D. G. Mitchell, Retrieval of global magnetospheric ion distributions from high-energy neutral atom measurements made by the IMAGE/HENA instrument, *J. Geophys. Res.*, *109* (A04214), doi:10.1029/2003JA010322, 2004.

Dessler, A. J. (Ed.), *Physics of the Jovian Magnetosphere*, Cambridge University Press, 1983.

Dessler, A. J., Differential rotation of the magnetic fields of gaseous planets, *Geophys. Res. Lett.*, *12* (5), 299–302, doi:10.1029/GL012i005p00299, 1985.

Divine, N., and H. B. Garrett, Charged particle distributions in jupiter's magnetosphere, *J. Geophys. Res.*, *88* (A9), 6889–6903, 1983.

Dougherty, M. K., A. Balogh, D. J. Southwood, and E. J. Smith, Ulysses assessment of the Jovian planetary field, *J. Geophys. Res.*, *101* (A11), 24,929–24,941, doi:10.1029/96JA02385, 1996.

Frank, L. A., and W. R. Paterson, Survey of thermal ions in the Io plasma torus with the Galileo spacecraft, *J. Geophys. Res.*, *106* (A4), 6131–6149, doi:10.1029/2000JA000159, 2001.

Futaana, Y., S. Barabash, M. Holmström, and A. Bhardwaj, Low energy neutral atoms imaging of the Moon, *Planet. Space Sci.*, *54* (2), 132–143, doi:10.1016/j.pss.2005.10.010, 2006.

Futaana, Y., J.-Y. Chaufray, H. Smith, P. Garnier, H. Lichtenegger, M. Delva, H. Gröller, and A. Mura, Exospheres and energetic neutral atoms of Mars, Venus and Titan, *Space Sci. Rev.*, *162*, 213–266, doi:10.1007/s11214-011-9834-4, 2011.

Futaana, Y., et al., Empirical energy spectra of neutralized solar wind protons from the lunar regolith, *J. Geophys. Res.*, *117* (E5), E05005, doi:10.1029/2011JE004019, 2012.

Futaana, Y., S. Barabash, M. Wieser, C. Lue, P. Wurz, A. Vorburger, A. Bhardwaj, and K. Asamura, Remote energetic neutral atom imaging of electric potential over a lunar magnetic anomaly, *Geophys. Res. Lett.*, *40*, 262–266, doi:10.1002/grl.50135, 2013.

Galli, A., et al., Tailward flow of energetic neutral atoms observed at Venus, *J. Geophys. Res.*, *113*, E00B15, doi:10.1029/2008JE003096, 2008a.

Galli, A., et al., Tailward flow of energetic neutral atoms observed at Mars, *J. Geophys. Res.*, *113* (E12), E12012, doi:10.1029/2008JE003139, 2008b.

Gladstone, G. R., and D. T. Hall, Recent results from EUVE observations of the Io plasma torus and Jupiter, *J. Geophys. Res.*, *103* (E9), 19,927–19,933, doi:10.1029/98JE00823, 1998.

Goldstein, J., and D. J. McComas, Five years of stereo magnetospheric imaging by TWINS, *Space Sci. Rev.*, doi:10.1007/s11214-013-0012-8, 2013.

Grande, M., Investigation of magnetospheric interactions with the hermean surface, *Adv. Space Res.*, *19*(10), 1609–1614, 1997.

Grasset, O., et al., JUpiter ICy moons Explorer (JUICE): An ESA mission to orbit Ganymede and to characterise the Jupiter system, *Planet. Space Sci.*, *78* (0), 1–21, doi:10.1016/j.pss.2012.12.002, 2013.

Gruntman, M., Energetic neutral atom imaging of space plasmas, *Rev. Sci. Instrum.*, *68*, 3617, 1997.

Hansen, C. J., D. E. Shemansky, and A. R. Hendrix, Cassini UVIS observations of europa's oxygen atmosphere and torus, *Icarus*, *176* (2), 305–315, doi:http://dx.doi.org/10.1016/j.icarus.2005.02.007, 2005.Herbert, F., G. R. Gladstone, and G. E. Ballester, Extreme ultraviolet explorer spectra of the Io plasma torus: Improved spectral resolution and new results, *J. Geophys. Res.*, *106*(A11), 26,293–26,309, doi:10.1029/2000JA002501, 2001.

Herbert, F., N. M. Schneider, A. R. Hendrix, and F. Bagenal, Hubble space telescope observations of sulfur ions in the io plasma torus: New constraints on the plasma distribution, *J. Geophys. Res., 108*(A5), 1167, doi:10.1029/2002JA009510, 2003.

Hill, T. W., A. J. Dessler, and F. C. Michel, Configuration of the jovian magnetosphere, *Geophys. Res. Lett., 1*(1), 3–6, doi:10.1029/GL001i001p00003, 1974.

Hill, T. W., and F. C. Michel, Heavy ions from the Galilean satellites and the centrifugal distortion of the Jovian magnetosphere, J. Geophys. Res., 81, 4561, doi:10.1029/JA081i025p04561, 1976.

Hill, T. W., Corotation lag in Jupiter's magnetosphere: Comparison of observation and theory, *Science*, *207* (4428), 301–302, doi:10.1126/science.207.4428.301, 1980.

Itikawa, Y., and A. Ichimura, Cross sections for collisions of electrons and photons with atomic oxygen, *J. Phys. Chem. Ref. Data*, *19* (3), 637–651, doi:10.1063/1.555857, 1990.

Johnson, R. E., and D. F. Strobel, Charge exchange in the Io torus and exosphere, *J. Geophys. Res.*, *87* (A12), 10,385–10,393, doi:10.1029/JA087iA12p10385, 1982.

Kazama, Y., S. Barabash, A. Bhardwaj, K. Asamura, Y. Futaana, M. Holmström, R. Lundin, R. Sridharan, and P. Wurz, Energetic neutral atom imaging mass spectroscopy of the moon and mercury environments, *Advances in Space Research*, *37* (1), 38–44, doi:doi: 10.1016/j.asr.2005.05.047, 2006.

Kim, Y. K., and J. P. Desclaux, Ionization of carbon, nitrogen, and oxygen by electron impact, *Phys. Rev. A*, *66*, 012708, doi:10.1103/PhysRevA.66.012708, 2002.

Kirsch, E., S. M. Krimigis, J. W. Kohl, and E. P. Keath, Upper limits for X-Ray and energetic neutral particle emission from Jupiter: Voyager-1 results, *Geophys. Res. Lett.*, *8* (2), 169–172, doi:10.1029/GL008i002p00169, 1981.

Kivelson, M. G., F. Bagenal, W. S. Kurth, F. M. Neubauer, C. Paranicas, and J. Saur, Magnetospheric interactions with satellites, in *Jupiter: The Planet, Satellites and Magnetosphere*, chap. 21, pp. 513–536, Cambridge University Press, 2004.

Krimigis, S. M., T. P. Armstrong, W. I. Axford, C. O. Bostrom, C. Y. Fan, G. Gloeckler, and L. J. Lanzerotti, The low energy charged particle (LECP) experiment on the Voyager spacecraft, *Space Sci. Rev.*, *21*, 329–354, doi:10.1007/BF00211545, 1977.

Krimigis, S. M., et al., A nebula of gases from Io surrounding Jupiter., *Nature*, *415* (6875), 994–996, doi:10.1038/415994a, 2002.

Kupo, I., Y. Mekler, and A. Eviatar, Detection of ionized sulfur in the Jovian magnetosphere, *ApJ, 205*, L51–L53, doi:10.1086/182088, 1976.

Lindsay, B. G., and R. F. Stebbings, Charge transfer cross sections for energetic neutral atom data analysis, *J. Geophys. Res.*, *110* (A12), doi:10.1029/2005JA011298, 2005.

Massetti, S., S. Orsini, A. Milillo, A. Mura, E. De Angelis, H. Lammer, and P. Wurz, Mapping of the cusp plasma precipitation on the surface of mercury, *Icarus, 166*(2), 229–237, 2003.

Mauk, B. H., D. G. Mitchell, S. M. Krimigis, E. C. Roelof, and C. P. Paranicas, Energetic neutral atoms from a trans-Europa gas torus at Jupiter, *Nature*, *421* (6926), 920–922, doi:10.1038/nature01431, 2003.

McComas, D., et al., IBEX—Interstellar Boundary Explorer, *Space Sci. Rev.*, *146* (1), 11–33, doi:10.1007/s11214-009-9499-4, 2009.

McGrath, M. A., and R. E. Johnson, Charge exchange cross sections for the Io plasma torus, *J. Geophys. Res.*, *94* (A3), 2677–2683, doi:10.1029/JA094iA03p02677, 1989.

McNutt, R. L., J. W. Belcher, J. D. Sullivan, F. Bagenal, and H. S. Bridge, Departure from rigid co-rotation of plasma in jupiter's dayside magnetosphere, *Nature*, *280* (5725), 803–803, doi:10.1038/280803a0, 1979.

Mendillo, M., J. Wilson, J. Spencer, and J. Stansberry, Io's volcanic control of Jupiter's extended neutral clouds, *Icarus, 170*(2), 430–442, doi:10.1016/j.icarus.2004.03.009, 2004.

Mendillo, M., S. Laurent, J. Wilson, J. Baumgardner, J. Konrad, and W. C. Karl, The sources of sodium escaping from Io revealed by spectral high definition imaging, *Nature, 448*(7151), 330–332, 2007.

Milillo, A., et al., Energetic neutral particles detection in the environment of jupiter's icy moons: Ganymede's and europa's neutral imaging experiment (genie), Planetary and Space Science, 88 (0), 53–63, doi:10.1016/j.pss.2013.08.008, 2013.

Nakano, S., G. Ueno, Y. Ebihara, M.-C. Fok, S. Ohtani, P. C. Brandt, D. G. Mitchell, K. Keika, and T. Higuchi, A method for estimating the ring current structure and the electric potential distribution using energetic neutral atom data assimilation, *J. Geophys. Res.*, *113* (A5), doi:10.1029/2006JA011853, 2008.

Nozawa, H., H. Misawa, S. Takahashi, A. Morioka, S. Okano, and R. Sood, Long-term variability of [SII] emissions from the io plasma torus between 1997 and 2000, *J. Geophys. Res., 109*(A7), A07,209, doi:10.1029/2003JA010241, 2004.

Orsini, S., A. Milillo, E. D. Angelis, A. M. D. Lellis, V. Zanza, and S. Livi, Remote sensing of mercury's magnetospheric plasma environment via energetic neutral atoms imaging, *Planet. Space Sci., 49* (14-15), 1659–1668, 2001.

Orsini, S., S. Livi, K. Torkar, S. Barabash, A. Milillo, P. Wurz, A. M. Di Lellis, and E. Kallio, Serena: A suite of four instruments (ELENA, STROFIO, PICAM and MIPA) on board BepiColombo-MPO for particle detection in the Hermean environment, *Planet. Space Sci.*, *58* (1–2), 166–181, doi:10.1016/j.pss.2008.09.012, 2010.

Plainaki, C., A. Milillo, A. Mura, S. Orsini, and T. Cassidy, Neutral particle release from europa's surface, Icarus, 210(1), 385–395, 2010.

Rees, M. H., *Physics and Chemistry of the Upper Atmosphere*, Cambridge University Press, 1989.

Richards, P. G., J. A. Fennelly, and D. G. Torr, EUVAC: A solar EUV flux model for aeronomic calculations, *J. Geophys. Res.*, *99* (A5), 8981–8992, doi:10.1029/94JA00518, 1994.

Roelof, E., and D. Williams, The terrestrial ring current-from in situ measurements to global images using energetic neutral atoms, Johns Hopkins APL Technical Digest, 9, 144–163, 1988.

Saito, Y., J. A. Sauvaud, M. Hirahara, S. Barabash, D. Delcourt, T. Takashima, and K. Asamura, Scientific objectives and instrumentation of Mercury Plasma Particle Experiment (MPPE) onboard MMO, *Planet. Space Sci.*, *58* (1–2), 182–200, doi:10.1016/j.pss.2008.06.003, 2010.

Sandel, B. R., and A. L. Broadfoot, Discovery of an Io-correlated energy source for Io's hot plasma torus, *J. Geophys. Res.*, *87* (A4), 2231–2240, doi:10.1029/JA087iA04p02231, 1982.

Sandel, B. R., and A. J. Dessler, Dual periodicity of the Jovian magnetosphere, *J. Geophys. Res., 93*, 5487–5504, 1988.

Schaufelberger, A., et al., Scattering function for energetic neutral hydrogen atoms off the lunar surface, *Geophys. Res. Lett.*, *38*, L22202, doi:10.1029/2011GL049362, 2011.

Schmidtke, G., F. G. Eparvier, S. C. Solomon, W. K. Tobiska, and T. N. Woods, The TIGER (thermospheric–ionospheric geospheric research) program: Introduction, *Adv. Space Res.*, *37* (2), 194–198, doi:http://dx.doi.org/10.1016/j.asr.2005.02.088, 2006.

Schneider, N. M., J. T. Trauger, J. K. Wilson, D. I. Brown, R. W. Evans, and D. E. Shemansky, Molecular origin of Io's fast sodium, *Science*, *253* (5026), 1394–1397, doi:10.1126/science.253.5026.1394, 1991.

Schneider, N. M., and F. Bagenal, Io's neutral clouds, plasma torus, magnetospheric interaction, in *Io After Galileo: A new view of Jupiter's Volcanic Moon*, edited by R. M. C. Lopes and J. R. Spencer, pp. 265–286, Springer, 2007.

Smyth, W. H., and M. R. Combi, A general model for Io's neutral gas clouds. I - Mathematical description, *ApJ Suppl. Ser.*, *66*, 397–411, doi:10.1086/191264, 1988.

Smyth, W. H., Neutral cloud distribution in the Jovian system, *Adv. Space Res.*, *12* (8), 337–346, 1992.

Smyth, W. H., and M. Marconi, Nature of the iogenic plasma source in Jupiter's magnetosphere I. Circumplanetary distribution, *Icarus*, *166* (1), 85–106, doi:10.1016/S0019-1035(03)00176-3, 2003.

Steffl, A. J., A. I. F. Stewart, and F. Bagenal, Cassini UVIS observations of the Io plasma torus: I. initial results, *Icarus, 172*(1), 78–90, doi: 10.1016/j.icarus.2003.12.027, 2004a.

Steffl, A. J., F. Bagenal, and A. I. F. Stewart, Cassini UVIS observations of the Io plasma torus: II. radial variations, *Icarus, 172*(1), 91–103, doi: 10.1016/j.icarus.2004.04.016, 2004b.

Steffl, A. J., P. A. Delamere, and F. Bagenal, Cassini UVIS observations of the Io plasma torus: III. observations of temporal and azimuthal variability, *Icarus, 180* (1), 124–140, doi:10.1016/j.icarus.2005.07.013, 2006.

Steffl, A. J., P. A. Delamere, and F. Bagenal, Cassini UVIS observations of the Io plasma torus: IV. modeling temporal and azimuthal variability, *Icarus, 194* (1), 153–165, doi: 10.1016/j.icarus.2007.09.019, 2008.

Thomas, N., F. Bagenal, T. W. Hill, and J. K. Wilson, The Io neutral clouds and plasma torus, in *Jupiter: The Planet, Satellites and Magnetosphere*, chap. 23, pp. 561–591, Cambridge University Press, 2004.

Wang, K., R. M. Thorne, R. B. Horne, and W. S. Kurth, Cold torus whistlers: An indirect probe of the inner jovian plasma- sphere, *J. Geophys. Res. 103*, 14 987-14 994, 1998a.

vVang, K., R. l'vi. Thorne, R. B. Horne, and W. S. Kurth, Constraints on jovian plasma properties from a dispersion analysis of unducted whistlers in the warm Io torus, *J. Geophys. Res. 103*, 14 979-14 986, 1998b.

Wieser, M., et al., Extremely high reflection of solar wind protons as neutral hydrogen atoms from regolith in space, *Planet. Space Sci.*, *57*, 2132–2134, doi:10.1016/j.pss.2009.09.012, 2009.

Wilson, J., M. Mendillo, J. Baumgardner, N. Schneider, J. Trauger, and B. Flynn, The dual sources of Io's sodium clouds, *Icarus*, *157* (2), 476–489, doi:10.1006/icar.2002.6821, 2002.

Wurz, P., Detection of energetic neutral particles, in *The Outer Heliosphere: Beyond the Planets*, edited by K. Scherer, H. Fichtner, and E. Marsch, pp. 251–288, Copernicus Gesellschaft e. V., Katlenburg-Lindau, 2000.

Yoneda, M., M. Kagitani, and S. Okano, Short-term variability of jupiter's extended sodium nebula, *Icarus, 204*(2), 589–596, doi: 10.1016/j.icarus.2009.07.023, 2009.

Yoneda, M., H. Nozawa, H. Misawa, M. Kagitani, and S. Okano, Jupiter's magnetospheric change by Io's volcanoes, *Geophys. Res. Lett., 37*(11), L11,202, doi:10.1029/2010GL043656, 2010.

Yoneda, M., et al., Mid-infrared observations of Io's volcanism from the ground in 2011 and 2012, *Icarus, 236*, 153–156, doi: 10.1016/j.icarus.2014.01.019, 2014.

Zarka, P., J. Queninnec, and F. J. Crary, Low-frequency limit of jovian radio emissions and implications on source locations and Io plasma wake, *Planet. Space Sci. 49*, 1137-1149, 2001.

Appendix A: ENA flux calculation under the influence of a gravity field

The ENA flux, j_{ENA}[cm^{-2} s^{-1} sr^{-1} eV^{-1}] is normally calculated as a line-of-sight integral of ENA generation:

$$j_{\mathrm{ENA}}(E) = \int_{-\infty}^{0} j_{\mathrm{plasma}}(E, \hat{l}) \cdot N_n(l) \cdot \sigma \cdot dl \qquad \text{(A1)}$$

where, j_{plasma} denotes the differential flux of plasma, E is the energy, l is the distance along the direction of flight of the ENAs, and $\hat{l}$ is the unit vector thereof. N_n and σ are the density of the neutral atoms and the cross section for the charge-exchange process, respectively. Equivalently, one may use the velocity distribution function, f_{ENA} [s^3/m^6], for the following formulation:

$$f_{\mathrm{ENA}}(\vec{v}) = \int_{-\infty}^{0} f_{\mathrm{plasma}}(v, \hat{l}) \cdot N_n(l) \cdot \sigma \cdot dl \qquad \text{(A2)}$$

where v is the velocity vector of the ENAs and v is their speed. f_{plasma} is the velocity distribution function of the plasma. In the following, the Expression (A2) is preferentially applied because although the velocity distribution functions are conserved by the translation of reference frames in velocity space, the differential flux is not.

Expressions of (A1) and (A2) can be used under the following assumptions: 1. the change in energy and direction during the charge exchange is negligibly small, 2. there is no loss of ENAs during the flight, 3. the observer is stationary, and 4. the trajectories of the ENAs are straight. The first assumption is, in most of the higher energy range, satisfied for the LENA case. For low energy images (say <30 eV), one has to in theory modify the energy loss and directional change to calculate the ENA flux. Under this circumstance, due to the angular spread, the image will be more "blurred". It is also noted that this effect should be visible in the frame moving together with the target neutrals. In the Io tori imaging case, the observer (spacecraft) is moving with respective to the Io neutral torus, the blurring effect will be less significant. In addition, the main peak of the Io tori ENAs is >100 eV for S and O, we neglect the energy loss and the directional change. The second assumption is not trivially negligible, but it is insignificant for Io-tori imaging (see section 3.2). To satisfy the third assumption, one should properly compensate for the spacecraft velocity (to be discussed below). The final assumption may be violated in the case of the Io torus imaging. The trajectories of low-speed LENAs are bent by the gravity of Jupiter, so (A2) should be modified.

Because no centrifugal nor Corioli's forces contribute explicitly, an inertial frame is used for the formulation. Under a gravitational field, the ENA production should be assessed along a ballistic trajectory. For the spacecraft position $\vec{r}_0$ and ENA velocity $\vec{v}_0$ to be observed, the ENA trajectory, $L = L(\vec{r}_0, \vec{v}_0)$, can be derived uniquely from the integral (backward in time) of the Newtonian equation of motion.

Let us now consider a small path length, dl, at a distance of l along the trajectory L. The position ($\vec{r}_1$) and velocity ($\vec{v}_1$) at distance l are determined by integrating the Newtonian equation of motion. Both are functions of l, namely,

$\vec{r}_1 = \vec{r}_1(l)$ and $\vec{v}_1 = \vec{v}_1(l)$. The time at *l* is also determined from the Newtonian equation of motion: $t_1 = t_1(l)$. Because the flying time of the ENA from the generation point to the spacecraft is typically several hours, which cannot be disregarded considering the time scale of the change in the environment (corotation is ~10 hours), the simulation must consider that ENA arriving at time t_0 are generated at different timing (t_1) along the ballistic trajectory depending on *l*. The ENA flux production, df_{ENA}, from this path length, d*l* ,is then

$$df_{\mathrm{ENA}}(\vec{r_1}, \vec{v_1}; t1) = f_{\mathrm{plasma}}(\vec{r_1}, \vec{v_1}; t1) \cdot \sigma \cdot N_n(\vec{r_1}; t_1) dl \qquad \text{(A3)}$$

All quantities should be calculated at time of t_1. We assume no energy loss during the charge exchange, namely, the source plasma velocity is also $\vec{v}_1$.

According to the Liouville theorem, the distribution function along the orbit is conserved. Thus, the integration of (A3) over the distance *l* yields the total ENA flux along the trajectory *L*.

$$f_{\mathrm{ENA}}(\vec{r}_0,\vec{v}_0;t_0=0) = \int \mathrm{d}f_{\mathrm{ENA}}(\vec{r}_1,\vec{v}_1;t_1) = \int_{-\infty}^{0} f_{\mathrm{plasma}}(\vec{r}_1,\vec{v}_1;t_1)\cdot \sigma \cdot N_n(\vec{r}_1;t_1)\mathrm{d}l \qquad \text{(A4)}$$

Expression (A4) describes the ENA velocity distribution function. A spacecraft is typically moving in an inertial frame, so the spacecraft velocity should be considered. We define the spacecraft (SC) coordinate system that moves with the spacecraft velocity, $\vec{V}_{\mathrm{sc}}$. The velocities in the inertial ($\vec{v}$) and SC ($\vec{v}'$) frames are related as follows: $\vec{v}' = \vec{v} + \vec{V}_{\mathrm{sc}}$. The velocity distribution function does not depend on the frame of the reference: $f(\vec{r},\vec{v}) = f'(\vec{r}',\vec{v}')$. Thus, the ENA velocity distribution function observed at the spacecraft can be described as

$$f'_{\mathrm{ENA}}(\vec{r}'_0=0,\vec{v}'_0;t=0) = f_{\mathrm{ENA}}(\vec{r}_0,\vec{v}_0;t=0)$$

The differential flux to be observed can be derived from the velocity distribution function.

$$j'_{\mathrm{ENA}}(\vec{r}'_0=0,E'_0,\Omega'_0) = \frac{2E'_0}{m^2} f'_{\mathrm{ENA}}(\vec{r}'_0=0,\vec{v}'_0) = \frac{2E'_0}{m^2} f_{\mathrm{ENA}}(\vec{r}_0,\vec{v}_0)$$

Here, energy and direction (E_0', Ω'_0) can be calculated from $\vec{v}_0{}'$ (and vice versa), and *m* is the mass of ENAs. In the rightmost expression, the energy is given in the SC frame (E_0').

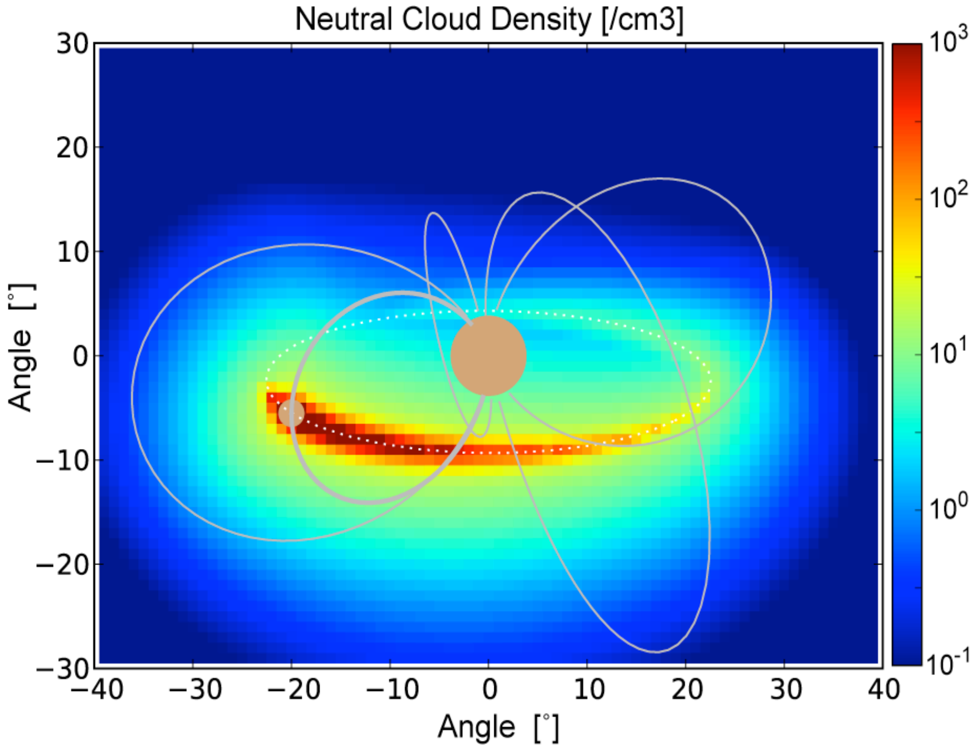

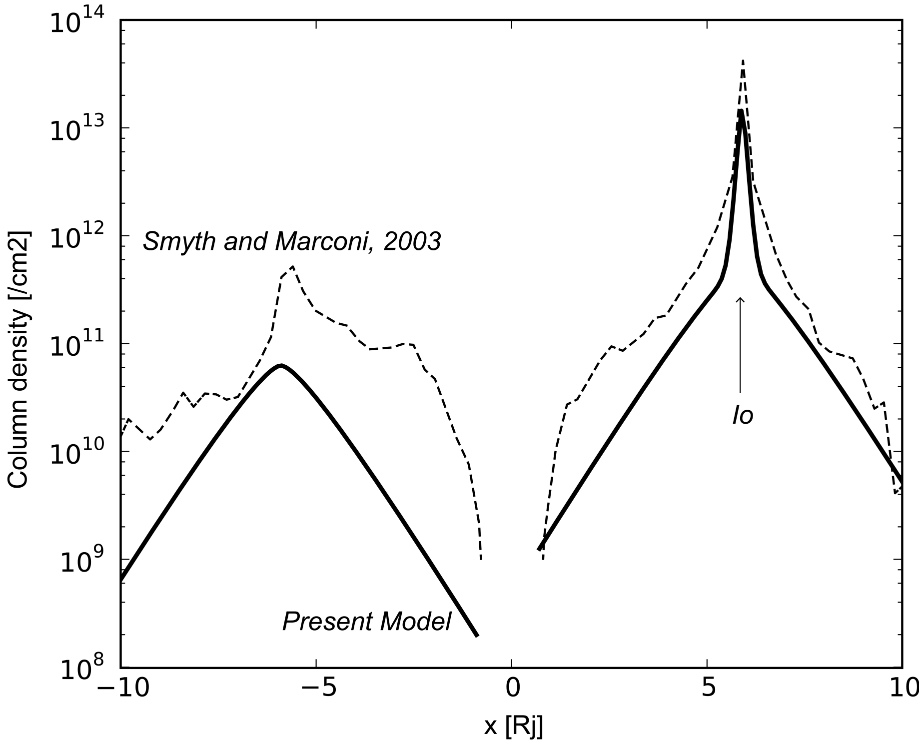

Figure 1: a) *Image of the density model of the Io neutral torus used in this paper. A virtual spacecraft was placed at ~15 Rj from Jupiter. The spacecraft is above the equatorial plane at ~16° north. The dipole magnetic field lines (L=10) are shown as thin gray lines. The field line that is connected to Io (small circle; not to scale) is depicted with a thick line. Jupiter, located at the center, is drawn to*

scale. ***b)*** *Comparison of our model (thick line) and the result obtained by Smyth and Marconi (2003; dashed line). The column density integrated along the z-axis (perpendicular to the Io orbital plane) is shown as a function of the Jupiter-Io distance along the Jupiter-Io line.*

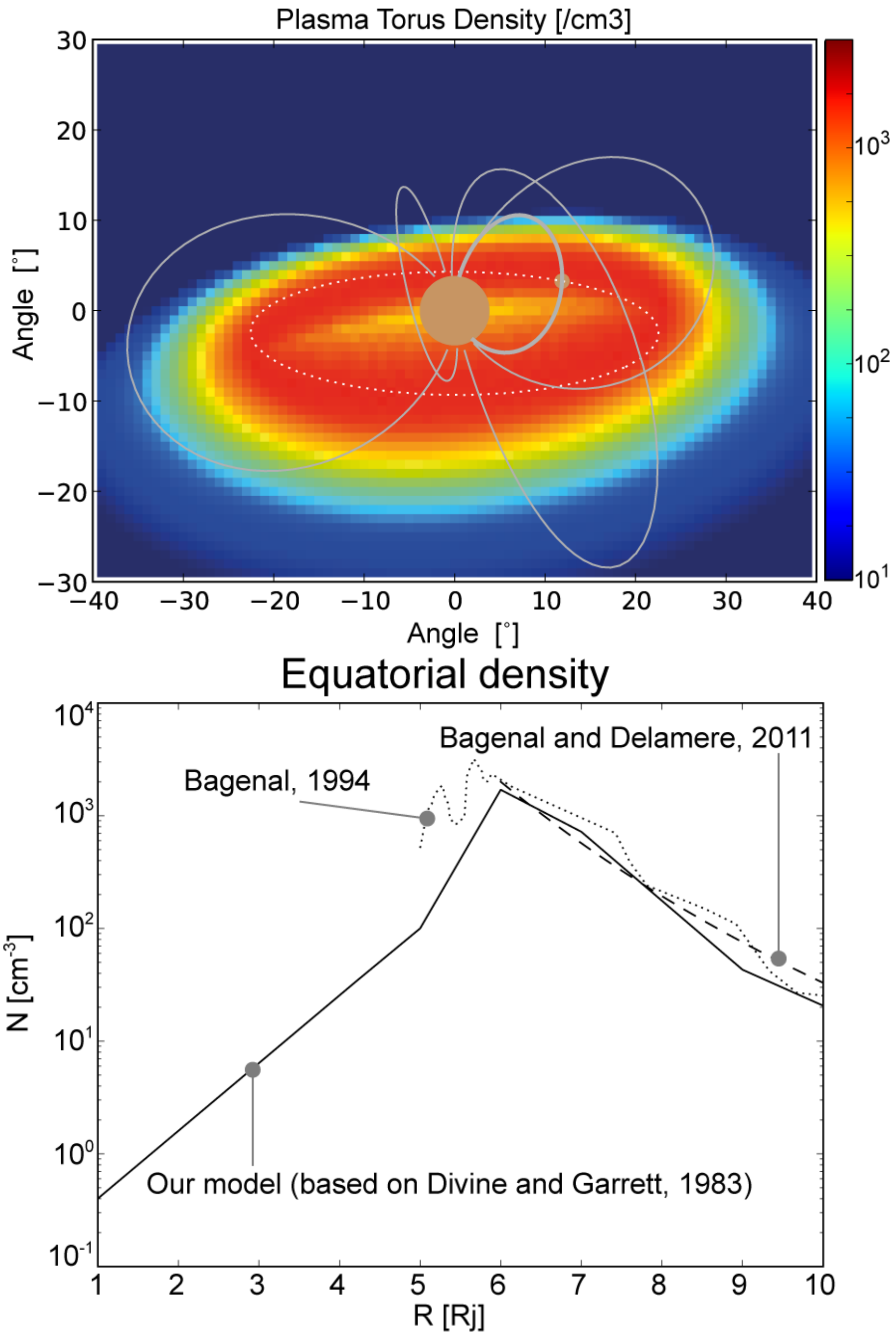

Figure 2: *a) Plasma density employed in the plasma-torus model in the same format as Figure 1a. b) The plasma density at the centrifugal equator as a function of the distance from the Jovian center. For comparison, two models (Bagenal,1994 and Bagenal and Delamere, 2011) are shown.*

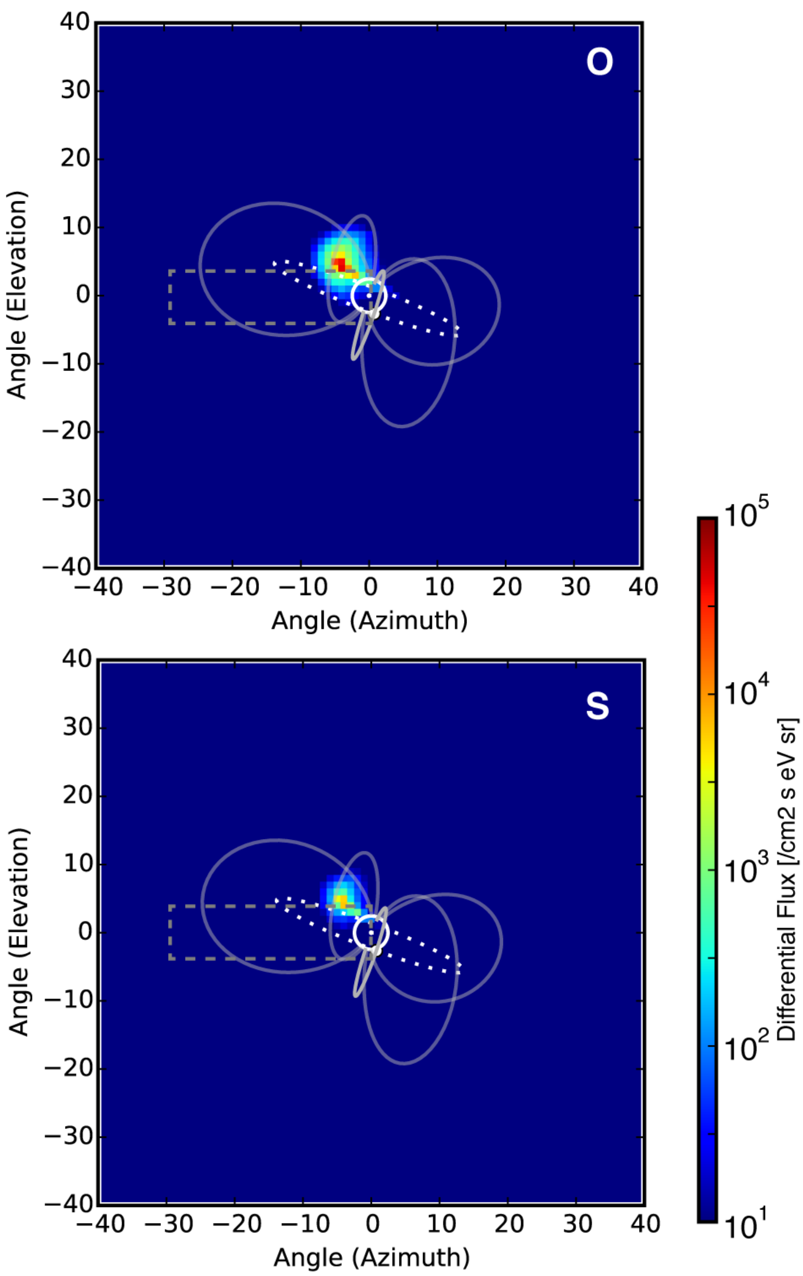

Figure 3: *The expected oxygen and sulfur LENA images for an energy of 210 eV and 420 eV. The spacecraft was located at 23.3 Rj at a latitude of 6.5° north from the Jovian equatorial plane as an example. The spacecraft-Io-Jupiter line is nearly co-aligned in the projection plane (Jupiter equatorial plane). The open circle at the origin is Jupiter (to scale). The thin gray curves are Jupiter's magnetic field lines for L=10. The location of Io at the time of observation is indicated by the filled circle in front of Jupiter, but it is not to scale; the real size of Io is considerably smaller. The magnetic field line of Jupiter that crosses the body of Io is represented by the white curve. The dotted white circle*

corresponds to the Io orbit. The sensor's field of view (see Table 2), which is used for Figure 5, is indicated by the gray dotted rectangle.

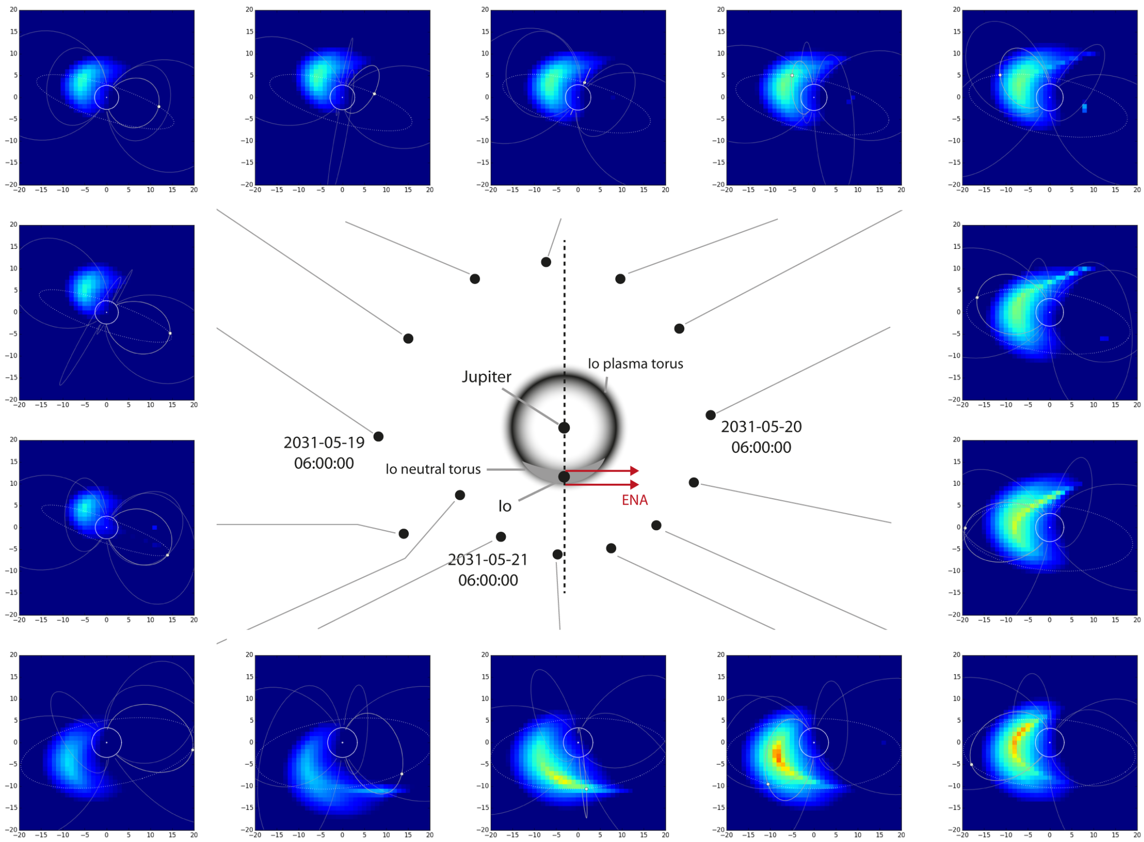

Figure 4: *Time series of simulated oxygen LENA images with energy of 210 eV. Illustration at the center is the geometry of the calculation. The Jupiter-centered Io fixed frame is used. In this frame, the LENA is emitted always in the same direction (red arrows). Spacecraft location every 4 hours are depicted by filled dots. Each panel shows the LENA image in the same format as Figure 3, but zoomed into 20x20 degrees.*

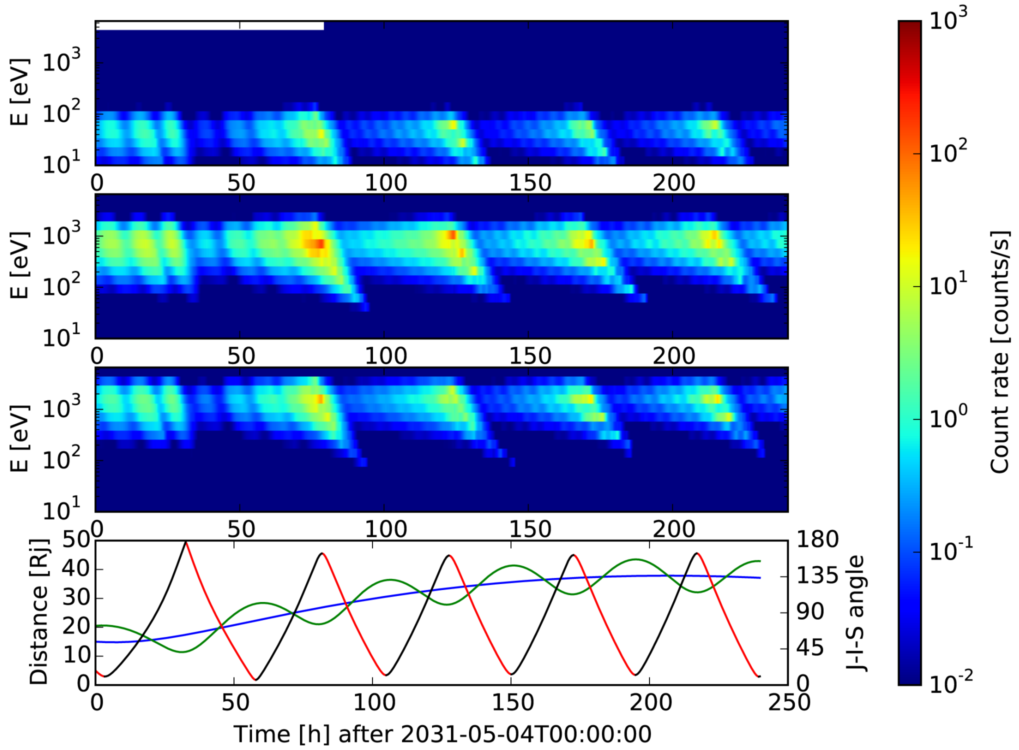

Figure 5: *a-c) Calculated energy-time spectrograms for three species of LENAs (H, O, and S). The preliminary JUICE orbit and the geometric factor of the JNA-prototype are used to calculate the count rates. A sensor pixel of 30x5° is used (see white box in Figure 3). d) The geometry of the spacecraft, Io, and Jupiter. The blue and green solid lines are the distances of the spacecraft from Jupiter and Io, respectively. The black and red solid lines represent the Jupiter-Io-spacecraft angle. A black (red) line indicates that Io is located on the toward (away) side, as seen from the spacecraft.*

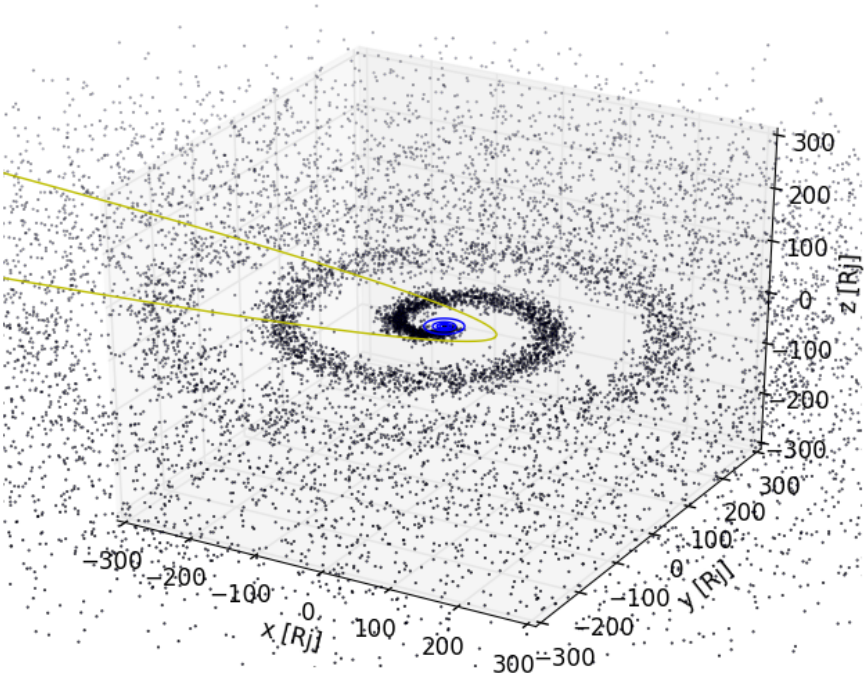

Figure 6: *A snapshot of a 3-D view of the spatial distribution of LENAs from the Io torus. Each dot represents a charge-exchanged LENA. The four blue circles in the center correspond to the orbits of the Galilean moons (the innermost circle corresponds to Io). A very simplified shape of the Jovian magnetopause (in the equatorial plane of Jupiter) is shown for reference.*

Table 1: *Charge-exchange cross sections in the units of 10^{-16} cm^2 for each plasma species at a relative velocity of ~60 km/s. For hydrogen- and proton-related reactions, we refer to Lindsay and Stebbings (2005). For other reactions, data from McGrath and Johnson (1989) are used. The convolved cross section for each ion species are first calculated by taking the weighted average of the neutral species. Then, taking the weighted average the relative fraction of the parent ion species in different charge state, the total cross section for each LENA species are calculated. Reactions for which cross sections are unavailable are disregarded for the calculation of total cross sections.*

	H	**O**	**S**	**O2**	**SO**	**SO2**	**Convolved cross section**	**Fraction**	**Total cross section**
H+	39	11		10			11.8	0.1	11.8
O+	11	22	11.2	13	1.6	11	18.9	0.4	18.8
O++		9.86	39				14.1	0.01	
S+		0	29	0	50	0	5.2	0.1	8.8
S++		12.15	13.5				11.2	0.15	
Fraction	0.56	4	1	0	0	0			

***Table 2**: Specifications of the LENA sensor (JNA-prototype) used to calculate the count rate from the physical quantities. The parameters are based on the predecessor sensors of the JNA-prototype, namely, ENA, mounted on BepiColombo/MMO and CENA mounted on Chandrayaan-1 (Kazama et al., 2006; Barabash et al., 2009).*

Angular resolution	30°x5°
Aperture	150°x7°
Energy range	10–3000 eV
Mass resolution	H, He, O, S, >S
Geometric factor (incl. efficiency)	5×10^{-5} cm^2 sr eV/eV
Energy resolution (DE/E)	100%

Table 3: *Characteristic quantities that can be retrieved from Io-torus LENA imaging.*

	Absolute value	Short-term (abrupt) variation	Long-term variation
Plasma torus			
Density	Convolved (line of sight (LOS) integral)	Instantaneous relative (velocity distribution function (VDF) shape change)	With difficulty
Velocity	Instantaneous (LOS weighted)		
Temperature	Instantaneous (LOS weighted)		
Composition (Species)	Instantaneous (LOS weighted)		
Composition (Charge state)	Possibly instantaneous (via velocity distribution function?)		
Neutral torus			
Density	Convolved (LOS integral)	Instantaneous relative (VDF shape invariant)	With difficulty
Velocity	No		
Temperature	No		
Composition	No or with difficulty (via cross section?)		

1205